JOURNAL OF SOLID STATE CHEMISTRY 25, 169–178 (1978)

Determination of Coordination Site and Oxidation States of Iron in Sodium β-Alumina through the Use of Mössbauer, Absorption, and Emission Spectroscopy, and Magnetic Susceptibility

J. R. AKRIDGE,*‡ B. SROUR,† C. MEYER,† Y. GROS,† AND J. H. KENNEDY,*§

**Department of Chemistry, University of California, Santa Barbara, California 93106 and †Laboratoire de Spectrometrie Physique, B.P. 53, 38041 Grenoble-Cedex, France*

Received October 28, 1977; in revised form, December 22, 1977

The absorption spectrum, emission spectrum, Mössbauer spectrum, and magnetic susceptibility for iron-doped β-alumina have been recorded for samples prepared in oxidizing and reducing atmospheres. Significant differences are noted for the two preparation atmospheres. Samples prepared by firing in air contain iron in both 2+ and 3+ oxidation states even though 3+ is the only state initially present. Samples fired under reducing conditions contain only 2+ iron. The four different techniques used to investigate oxidation state and site symmetry for iron in β-alumina agree on the assignment of both 2+ and 3+ iron to tetrahedral coordination sites in β-alumina

Introduction

β-alumina is presently under intensive study for use in the sodium–sulfur cell. In our laboratory we have been investigating the properties of β-alumina doped with the first series transition metals. Many investigations are currently underway to determine oxidation state and coordination site for metals doped into the β-alumina lattice (*1–3*). Most investigators utilize single crystal β-alumina grown via inductive heating or other methods which incorporate the desired dopant into β-alumina in the molten state. Ion exchange methods at low temperature are also used (*4*). Although these methods of incorporating various dopants into β-alumina generally provide the desired material for study these methods can be very different from incorporating dopants via normal reactive sintering. However, sintering of powders containing the dopant for study provides polycrystalline sinters and not single crystals. Accordingly, methods have been developed to record absorption spectra directly through polycrystalline sinters or powders prepared from sinters. The results obtained from β-aluminas incorporating transition metal impurities prepared via normal sintering techniques used for undoped β-alumina are thought to provide more representative information on the resulting site symmetry and oxidation states of impurities than melting and/or ion exchange techniques. Indeed, the methods used in this investigation are thought to be applicable to the study of any polycrystalline material for the recording of absorption

‡ On leave at: I.N.P.G.–E.N.S.E.E.G., Laboratoire d'Energetique et Electrochimique, L.A. 265, Domaine Universitaire, B.P. 44, 38401 Saint Martin d'Heres, France.

§ Author to whom correspondence should be addressed.

0022–4596/78/0252–0169$02.00/0

spectra provided the material can be prepared so that it is translucent. Single crystals, of course, still provide high quality spectra but the methods used to prepare single-crystal material can be quite different from the methods used to prepare materials for general commercial use. The thermal history of a sample can be an important factor in the resulting site symmetry and oxidation state of impurities.

Experimental

β-alumina was doped with approximately 2 w/o iron by adding $Fe(NO_3)_3 \cdot 6H_2O$ to Alcoa XB-2 "Super Ground" β-alumina in an acetone slurry. The β-alumina plus metal nitrate was thoroughly mixed using an α-alumina mortar and pestle. The acetone was evaporated by directing a stream of compressed air into the mortar. When the powder was free of solvent, further mixing was performed to break up the β-alumina lumps formed upon solvent evaporation. The β-alumina plus metal nitrate was then placed in an α-alumina crucible with cover and calcined in air at 1000°C for 16 hr to decompose the nitrate.

The calcined powder was then cold pressed in a KBr pellet die using a bench laboratory press, packed in 300 mesh β-alumina and sintered in air at 1600° for 3 hr in an Astro Ind., Inc., Model 1000A Ultra High Temperature furnace. Samples from this sintering were also heated in an atmosphere of 10% H_2/90% N_2 for 5 hr at 1200°C to determine the effect, if any, on oxidation states of iron. The pellets of β-alumina were well packed with 300 mesh β-alumina for this heating. X-ray powder diffraction was performed on all materials and confirmed the absence of α-Al_2O_3 in the samples investigated.

Absorption spectra were recorded in two ways. Samples sintered in air were ground into very fine powder and then mixed with spectroscopic grade KBr. The procedure for the forming of pellets is reported in the literature (*5*). The absorption spectrum of iron was recorded through these pellets using a Cary Model 15-UV-Visible spectrophotometer over the wavelength 260 to 700 nm. Only one absorption band could be found for air sintered material by using KBr disks (Fig. 5). The attempt to record the absorption spectrum of sinters which had been reductively heated was unsuccessful with KBr disks. It was thought that bands were missing for air-fired material and that the KBr technique was inadequate. A photographic technique was then developed using a Glass–Bass Kessler spectrograph[1] and disks of sintered β-alumina in massive form without the necessity of powdering or mixing with another material to record the absorption spectrum (Fig. 1).

The Glass Bass–Kessler spectrograph is a grating instrument with 25 Å/mm dispersion and 10 Å resolution using a 250-μm slit. The spectra for air-fired and reductively fired material were photographed using Kodak Plus-X pan professional 4 × 5 in. sheet film.

[1] Designed by H. P. Broida and S. E. Johnson, both members of the Department of Physics, University of California, Santa Barbara, Calif. 93106.

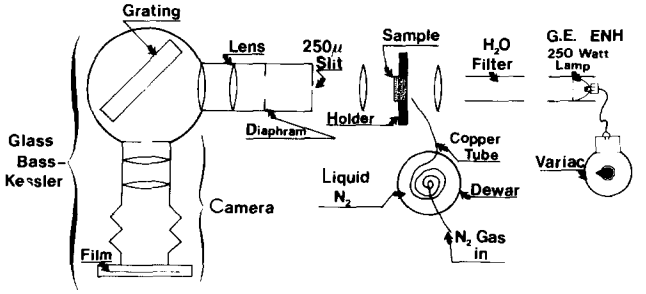

FIG. 1. Apparatus for the photographic recording of absorption spectra.

Spectra were calibrated by superimposing mercury emission bands on each exposure—eight exposures per film sheet. Absorptions were indexed by measurement of their position from Hg bands. Spectra were recorded at 77°K and room temperature using the apparatus of Fig. 1.

Emission spectra were obtained at 77°K using a 1000-W xenon lamp and monochromator to produce 365-nm exciting radiation. Emission was scanned from 9000 to 25 000 cm^{-1} using a Perkin–Elmer Model 98 prism monochromator and an R.C.A. 7102 phototube cooled with dry ice. Spectra were recorded on a Rikadenki B-161 chart recorder. Spectra were corrected for phototube spectral response and monochromator spectral response by a program written for a Hewlett–Packard 9820 calculator.

Samples for magnetic susceptibility measurements were checked for ferromagnetic behavior by examining the susceptibility versus field strength. No ferromagnetic effects were found at 300°K. Susceptibility measurements were performed at 300°K by Dr. R. T. Lewis[2] using an instrument of his own design (*6*, *7*). The susceptibility versus temperature measurements were performed by Mr. R. Buder[3] using a vibrating sample magnetometer from 4.2 to 300°K with a constant field strength of 9560 G. All samples for measurement were carefully dried for 72 hr at 300°C. The analysis for dopant concentration necessary for the calculation of μ_{eff} was by colorimetric (*8*) and atomic absorption methods.[4] The Mössbauer samples contained 2.25w/o Fe for the reduced material. Material of 2.95 w/o was used for the air-fired or "oxidized" Mössbauer and magnetic measurements.

The Mössbauer spectrometer was designed and built by the authors (B.S., C.M., and Y.G.) for use at Laboratoire de Spectrometric Physique. The reference material was stainless steel. The cobalt-57 γ-ray source was contained in a rhodium matrix. Each sample was counted for several hours using a multichannel analyzer.

[2] Chevron Research Corporation, Richmond, Calif.

[3] Groupe des Transitions de Phase, C.N.R.S., B.P. 166, 38042 Grenoble, France.

[4] E.N.S.E.E.G. SERVICE LAREC, Domaine Universitaire, 38401 Saint Martin D'Hères, France.

Mössbauer Spectrum

The Mössbauer spectra of iron-doped β-alumina are shown in Fig. 2 for a sample fired in 10% H_2/90% N_2 after air sintering and Fig. 3 for a sample sintered in air. Figure 2 displays a well-defined quadrupole doublet. The spectrum of Fig. 3 is the superimposition of two quadrupole doublets: "a" has the same general characteristics as the spectrum of Fig. 2. The other, "b," has a different quadrupole splitting and isomer shift at room temperature. As the temperature decreases, the doublet b of Fig. 3 remains constant but the doublet a of Fig. 3 and the doublet of Fig. 2 for the two firing conditions show an important increase of the quadrupole splitting (Table I and Fig. 2). From these variations and from the respective isomer shifts, it can be deduced that the doublets of Figs. 2 and 3a belong to iron in a 2+ oxidation state and the doublet b of Fig. 3,

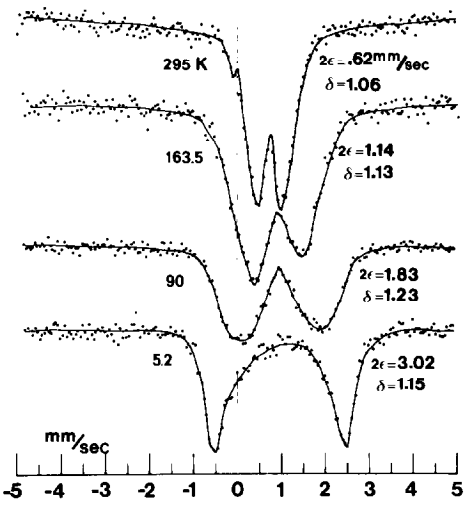

FIG. 2. Mössbauer spectrum of 2.25 w/o iron in β-alumina after firing in 10% H_2/90% N_2. Error limits for 2ε and δ: ±0.02 mm/sec.

whose quadrupole splitting has little temperature dependence, to a 3+ oxidation state.

The identification of the symmetry of the spinel sites occupied by iron requires some caution. Generally in a spinel the isomer shifts of Fe^{3+} and Fe^{2+} differ by approximately 0.15 mm/sec when symmetry changes from tetrahedral to octahedral (*9*, *10*). For example, in the spinels $FeCr_2O_4$, $FeAl_2O_4$, and $ZnCr_2O_4:Fe^{2+}$, where Fe^{2+} is present in tetrahedral sites, the isomer shifts are on the order of 1 mm/sec at room temperature, while in the spinels $GeFe_2O_4$, and $GeCo_2O_4:Fe^{2+}$, where Fe^{2+} is present in octahedral sites, their values are on the order of 1.2 mm/sec. In the present case, the δ values 1.06 and 1.07 mm/sec for the doublets of Figs 2 and 3a, respectively, are reasonably characteristic of Fe^{2+} in tetrahedral coordination.

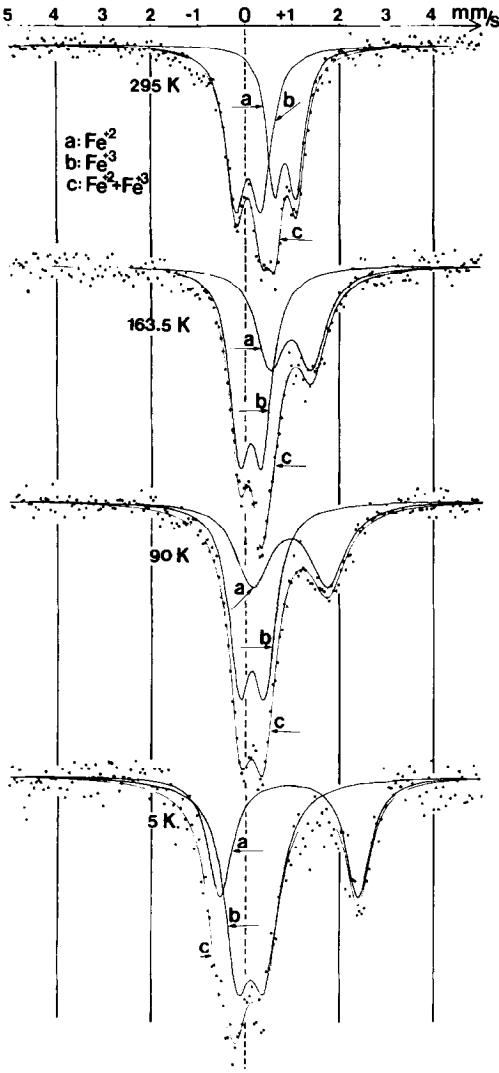

FIG. 3. Mössbauer spectrum of 2.95 w/o iron in β-alumina immediately following air sintering.

The spinels $ZnFe_2O_4$, $ZnCr_2O_4:Fe^{3+}$, $NiFe_2O_4$, and γ-Fe_2O_3, which have Fe^{3+} in octahedral symmetry, have isomer shifts near 0.45 mm/sec at room temperature. The spinels $NiFe_2O_4$ and γ-Fe_2O_3 also possess a tetrahedral Fe^{3+} whose isomer shift is around 0.35 mm/sec. The doublet b of Fig. 3, whose isomer shift is 0.3 mm/sec, then seems to be characteristic of Fe^{3+} also in tetrahedral coordination.

Another structural indication is given by the temperature dependence of the quadrupole splitting of the Fe^{2+} doublets of Figs. 2 and 3a. The quadrupole splitting values 2ε (Fig. 2 and Table I) plotted as a function of temperature are very well fitted with a hyperbolic tangent (tanh) dependence in $1/T$ according to the expression:

$$2\varepsilon = 2\varepsilon_0 \tanh(\Delta/2kT) \qquad \text{(Fig. 4)}$$

Such a variation of 2ε is characteristic of Fe^{2+} in tetrahedral site symmetry when the degeneracy of the orbital doublet E_g is lifted (*9*).

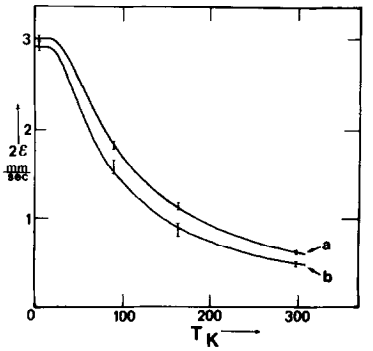

FIG. 4. Temperature dependence of the quadrupole splitting for Fe^{2+} in β-alumina. "a": 10% H_2/90% N_2 fired. "b": air fired.

TABLE I

QUADRUPOLE AND ISOMER SHIFT VALUES FOR SPECTRA OF FIGURE 3

	Fe^{2+}		Fe^{3+}	
T_K	Quadrupole splitting (2ε mm/sec)[a]	Isomer shift[d] (δ mm/sec)[b]	Quadrupole splitting (2ε mm/sec)[a]	Isomer shift[d] (δ mm/sec)[c]
295	0.49	1.07	0.52	0.30
163.5	0.88	1.20	0.47	0.33
90	1.60	1.18	0.53	0.35
5.2	2.93	1.20	0.58	0.40

[a] Error = $\pm$0.05 mm/sec.
[b] Error = $\pm$0.04 mm/sec.
[c] Error = $\pm$0.02 mm/sec.
[d] Reference is 310 stainless steel.

The energy separation between the two electronic singlets is Δ. On the contrary, in octahedral symmetry, the lowest orbital state, T_{2g}, would not lead to a tanh formula dependence. Notice that the above expression for 2ε is strictly valid only if Δ is much larger than the splitting due to spin–orbit coupling.

With E_g, the spin–orbit coupling appears as a second-order perturbation and in cubic symmetry it gives rise to an overall splitting of at most 60 cm^{-1} (R. Ingalls (*27*) gives an excellent description of the effect of the crystal field upon the quadrupole splitting); in the presence of a distortion, the tanh formula is, therefore, a fairly good approximation. The values of Δ deduced from experiment using this formula are 88 cm^{-1}, for the sample fired in 10% H_2/90% N_2, and 73 cm^{-1}, for the air-sintered sample. This gives a good demonstration of the tetrahedral nature of the site.

Finally, it can be noted that there is a slight asymmetry for the Mössbauer absorptions of Fig. 2. Notice that in the 295°K spectrum of Fig. 2 there is a very small absorption at about –0.2 mm/sec. This is due to a small residual of Fe^{3+} remaining in the sample. This absorption appears in an identical location for the 295°K spectrum of air-fired material (Fig. 3). The residual Fe^{3+} produces some asymmetry in the Mössbauer absorptions of Fe^{2+} in Fig. 2 at temperatures below 295°K.

Absorption Spectrum

The absorption spectra of air- and 10% H_2/90% N_2-fired samples are shown in Figs. 5 and 6. The absorption spectrum of air-fired samples is very simple consisting of two broad absorptions. The absorptions seen are rather surprising, however, since iron is known to be present in only the 2+ and 3+ oxidation states. Both of these oxidation states are known or expected to have very narrow absorptions arising from spin-forbidden transitions (*11*, *12*). The difficulty in the case of air fired material is that of overlapping absorptions from both oxidation states. The color of 2 w/o iron-doped air fired samples is grey which changes to light pink upon heating in a reducing atmosphere. The color change can be

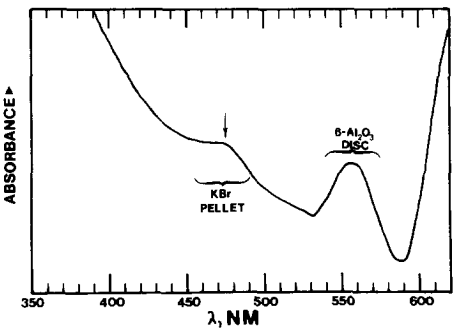

FIG. 5. Absorption spectrum of iron in β-alumina after air sintering.

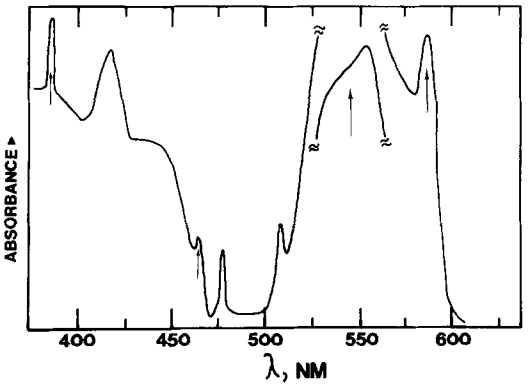

FIG. 6. Absorption spectrum of Fe^{2+} in β-alumina.

attributed to the removal of the 3+ absorption bands.

The assignment of the two air-fired bands has not been successful. However, the band centered at 558 nm in air-fired samples is perhaps the same absorption at that position in hydrogen-fired samples. It is unknown at present if it is possible to maintain iron in a 3+ oxidation state by sintering samples in pure oxygen.

The absorption spectrum of Fe^{2+} (Fig. 6) is due to spin-forbidden transitions from the $^5E(^5D)$ ground state to various triplet levels. A study of Fe^{2+} in spinel ($MgAl_2O_4$) has been performed by E. S. Gaffney (*12*). The absorptions observed in β-alumina in the present study are in excellent agreement with Gaffney's study. The Mössbauer and emission spectra and magnetic susceptibility measurements leave little doubt that the observed absorptions are those of Fe^{2+}. The triplet terms responsible for the absorption spectrum are difficult to assign.

The Tanabe–Sugano diagram for the triplet levels is complex. Gaffney assigned only the symmetry of the terms and made no assignment of the free ion terms giving rise to the triplet levels assigned. It is believed, in the present study, that without further extensive investigation into band intensity variations with iron concentration, the previous assignment can hardly be improved. This is not to say that the previous investigation has been proven but only that with the data for β-alumina presently available further improvement on band assignment is doubtful.

The absorbance for the observed bands is large. Due to the method used to obtain the absorption bands it is not possible to give an exact value of the extinction coefficient for any band. An estimate for the extinction coefficient of the band at 550 nm is 50 liter/mole-cm, which is as large as or greater than most spin allowed absorptions for 3*d* metals. This large extinction coefficient is also consistent with Fe^{2+} in tetrahedral geometry. The low site symmetry greatly relaxes the spin selection rule. Enhanced absorption for spin-forbidden bands in tetrahedrally coordinated metals is well known both from theory and experiment.

Emission Spectrum

The emission spectra of air- and 10% H_2/90% N_2-fired samples is shown in Fig. 7. The emission of air-fired material displays a very sharp, strong green emission and a very much weaker red band. The emission of 10% H_2/90% N_2 fired material displays only a triply structured red emission with no green emission detectable. The green emission for iron has been observed previously (*13–15*). Jaffe (*13*) attributed the green emission which he observed to tetrahedral site symmetry of Fe^{3+} in β-$LiAl_5O_8$. The evidence in the present study shows that this green emission must

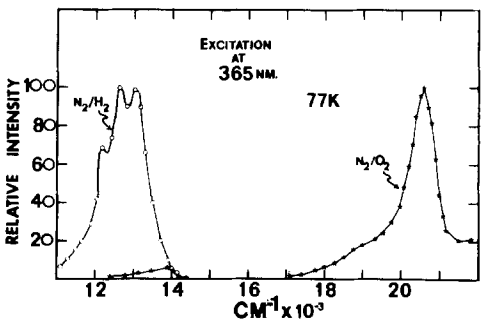

FIG. 7. Emission spectra of iron in β-alumina for the two different firing atmospheres.

certainly be from Fe^{3+} in tetrahedral symmetry in β-alumina. However, the relative intensities of the two peaks for air-fired samples are reversed from those reported by Jaffe. It should be noted that β-alumina has four crystallographically independent cation sites while spinel has only two such sites.

Fe^{3+} is a d^5 ion as is Mn^{2+}. The emission for Mn^{2+} in tetrahedral symmetry (*13*, *14*, *16*) is very similar in bandwidth and general appearance to that of the air-fired samples for the green emission band. One could expect that for ions with similar configurations and coordination symmetry to have very similar emission spectra. In addition, Mn^{2+} in β-alumina also gives a strong green emission very similar to air-fired iron samples. Mn^{2+} is known to be present in tetrahedral sites in β-alumina (*3*, *17*).

The weak red band for air-fired samples and the much stronger one for 10% H_2/90% N_2 fired samples are due to Fe^{2+} in tetrahedral site symmetry. As has been shown by Mössbauer spectroscopy, a mixture of 2+ and 3+ oxidation states occurs for iron upon air sintering. The increase in intensity for the red emission after reductive heating is most certainly due to the increase of emitting ions of 2+ oxidation state.

The triplet nature of the hydrogen-fired sample emission is probably a result of the lifting of the degeneracy of either the $^5T_2(^5D)$ or the $^3T_1(^3H)$ term due to low symmetry of the occupied site. The energy of the $^3T_1(^3H)$ term is around 14 000 cm^{-1} for Fe^{2+} in tetrahedral symmetry (*12*). The spin allowed $^5T_2(^5D)$ is expected to be around 4000 cm^{-1}. It is possible that Fe^{2+} in β-alumina could give rise to a red emission from its spin allowed $^5T_2(^5D)$ to the ground state ($^5E(^5D)$), but a definite assignment of the red emission origin cannot be made. However, a reasonable guess would be that the red emission arises from the $^3T_1(^3H)$ and not the $^5T_2(^5D)$ due to the latter's very low energy in this system.

Phosphorescent lifetime study of the red emission could help identify the correct emitting level for the red band. The lifetime of the $^5T_2(^5D)$ should be short since the emission from it to the ground state is spin allowed. The lifetime of the $^3T_1(^3H)$ should be longer since emission from it to the ground state is spin forbidden. The low site symmetry, however, may sufficiently lift the spin forbiddenness of the latter transition to make its half-life comparable to the spin-allowed transition.

Magnetic Susceptibility

The temperature dependence of the magnetic susceptibility and magnetic moment of iron for the two firing conditions is shown in Figs. 8, 9, and 10. The behavior of the susceptibility for both firing conditions obeys the Curie–Weiss law. The ground state of Fe^{2+} is ^5E and that of Fe^{3+} is $^6A_1$. Ions possessing A and E ground-state symmetry are expected to follow the Langevin–Debye Eq. (*18*). If Fe^{2+} were present in octahedral coordination, the ground state would be $^5T_2$. The susceptibility of ions possessing "T" ground terms is generally a complex function of temperature. The $^5T_2$ ground term, however, does not vary appreciably with temperature (*19*). This makes the distinction between octahedral and tetrahedral symmetry impossible to determine from magnetic measurements alone.

The behavior of the magnetic moment for Fe^{2+} is not ideal (Fig. 10). Some exchange phenomenon is possible at low temperatures resulting in the decrease of the moment at temperatures below 80°K. This is not unusual

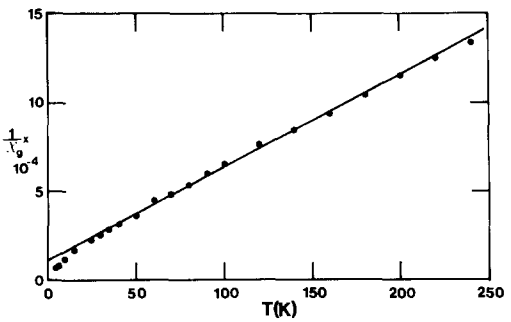

FIG. 8. Temperature dependence of the magnetic susceptibility of iron in β-alumina fired in air.

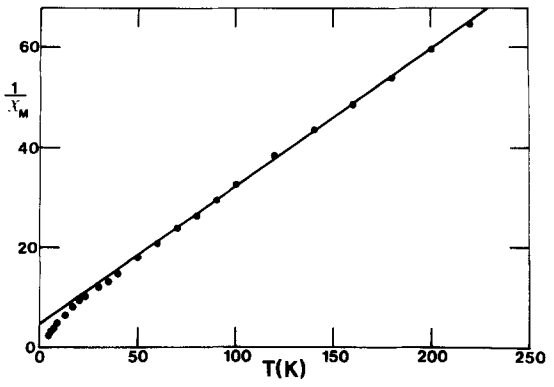

FIG. 9. Temperature dependence of the magnetic susceptibility of iron in β-alumina fired in 10% H_2/90% N_2.

since most paramagnetic species display magnetically concentrated behavior at low temperatures. β-alumina, being a very complex host lattice, could not be expected to yield magnetically ideal behavior for ions substituted within its lattice. At very low temperatures even small quantities of magnetic impurities or exchange phenomena will be important. The important result from the behavior of the magnetic moment is that above 80°K ($kT/\lambda \simeq 0.5$) the moment rises slowly until at 290°K ($kT/\lambda \simeq 2$) the moment is 5.33 B.M. The magnetic moment for octahedral Fe^{2+} is about 5.50 B.M. (*19*, *20*) at 290°K which is only slightly greater than observed here.

The magnetic measurements can not be considered in anyway as conclusive evidence for tetrahedral coordination for Fe^{2+} in β-alumina. The low site symmetry in β-alumina would cause the magnetic moment of an octahedrally coordinated iron to approach the spin-only value of 4.90 B.M. However, the magnetic moment of 5.33 B.M. at 290°K is further confirmation of a d^6 high spin state for Fe in samples fired in 10% H_2/90% N_2 atmosphere.

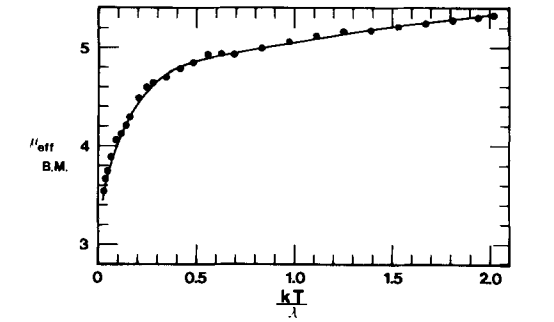

FIG. 10. Behavior of the magnetic moment of Fe^{2+} in β-alumina.

Discussion

The determination of oxidation states and lattice site occupancy for impurities in β-alumina is a matter of some importance. Impurity additions can be very powerful sintering and conductivity enhancers or inhibitors (*21*, *22*). The site occupied by ions of oxidation states different than 3+ can also have an influence of lattice strains in β-alumina. Roth (*23*) has given a very excellent description of this effect. In light of the reduction of lattice strains in β-alumina for the location of impurities of 2+ charge on the Al(2) (Ref. (*24*) and Fig. 11) lattice site, it is not surprising to find many 2+ ions substitute that site (*25*, *26*). The identification of tetrahedral coordination for iron in β-alumina for both Fe^{2+} and Fe^{3+} plus the knowledge of lattice site strain relief possible for 2+ ions on Al(2) sites, leads one to suspect that Fe^{2+} rests on the Al(2) site. The position of the 3+ ions including iron can be somewhat questionable.

There exists in β-alumina two tetrahedral sites (Fig. 11). When Fe^{3+} is reduced by heating in 10% H_2/90% N_2 there must be an electron transfer presumably from hydrogen to Fe^{3+}. It would seem that this transfer could be made to an Fe^{3+} situated on the Al(3) site more easily than if Fe^{3+} were located on the Al(2) site in the center of the spinel block. The charge compensation could then be an H^+ situated in the conducting plane close to Fe^{2+} on the Al(3) site perhaps bonded to or in conjunction with the 05 oxygen. Location of Fe^{3+} on the Al(3) site could satisfy three criteria: (1) The known preference of Fe^{3+} for tetrahedral coordination; (2) The net lowering of

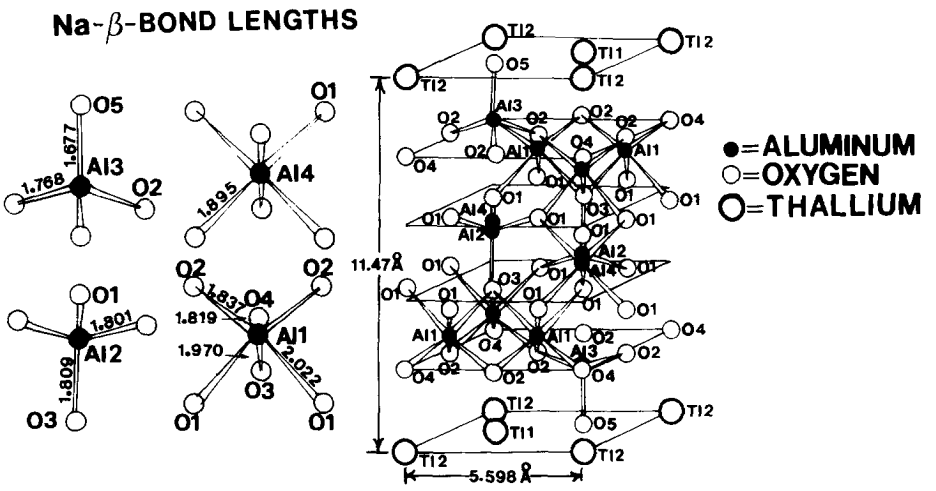

FIG. 11. Crystal structure of Tl-β-Alumina: C-axis projection. Taken from Ref. (*24*).

the lattice strain in β-alumina by the location of Fe^{2+} on Al(2) sites and Fe^{3+} on Al(3) sites. The possibility of translation of the 05 oxygen to relieve strain produced by a 3+ ion can provide a mechanism whereby the relief of strain on Al(2) sites is not cancelled out by locating another 3+ ion on a tetrahedral site where there is no mechanism to relieve the induced strain; (3) The electron transfer and subsequent charge compensation needed to reduce Fe^{3+} to Fe^{2+} with relative ease. This is, of course, only a suggestion.

Another possible mechanism for reduction utilizes an interstitial oxygen:

$$2Fe^{3+}_{Al(3)} + H_2 + O^{2-}_{inter} \rightarrow 2Fe^{2+}_{Al(3)} + H_2O\uparrow.$$

This second mechanism is probably the more likely of the two.

In contrast, it is also entirely possible for hydrogen to reduce a metal impurity located in the center of the spinel block as has been found for Cr^{4+} in β-alumina (*17*) where chromium occupies the Al(1) position (*1*). Further studies via NMR to determine if H^+ is present in the conducting planes and neutron-scattering or X-ray diffraction are necessary to determine exactly the location of iron in the β-alumina lattice.

Howe and Dudley (*28*) assigned, using magnetic measurements, Fe^{2+} in potassium ferrite ($K_{1+x}Fe_{11}O_{17}$) to the Al(4) or 2*a* sites in the compound. The 2*a* site is the octahedral site in the center (Fig. 11) of the spinel block. This is not what is found for sodium-β-alumina where Fe^{2+} is definitely present in tetrahedral coordination. Several other differences between ferrites and sodium-β-alumina are obvious. Howe and Dudley's spectra are complex. Each crystallographically different iron 3+ gives rise to magnetically split resonances in contrast to a quadrupole doublet for Fe^{3+} in β-alumina. The magnetic environment for iron 3+ in the ferrites is very similar to that in Fe_2O_3 which also gives a magnetically split sextuplet. The Fe 3+ environment in sodium-β-alumina is such that there is no magnetic dipole interaction to split the quadrupole doublet further. The charge compensating effect Fe^{2+} has for excess K^+ incorporated into the ferrite is similar to that of Fe^{2+} in sodium-β-alumina. Sodium-β-alumina plus Fe_2O_3 after sintering shows an increase in ionic con-

ductivity (*21*). This can be explained by the removal of oxide interstitials present in the conducting planes and/or the stabilization of extra sodium in those planes.

Conclusion

The four techniques used to investigate β-alumina doped with iron all show iron to exist in tetrahedral coordination in β-alumina. The oxidation states of iron produced depend upon firing atmosphere. β-alumina plus 2 w/o iron sintered in air contains both Fe^{2+} and Fe^{3+} in rather equal proportion even though only Fe^{3+} is initially present prior to sintering. Subsequent firing of the air-sintered material in 10% H_2/90% N_2 for 5 hr at 1200°C results in the reduction of Fe^{3+} to Fe^{2+}. Although it is not possible to definitely assign iron 2+ and 3+ to either the Al(2) or Al(3) tetrahedral sites, it has been suggested, in light of past work, that Fe^{2+} is most likely to be found in the Al(2) site. The site for Fe^{3+} can be either Al(2) or Al(3). Further work is needed to assign unambiguously which site(s) is occupied by iron in β-alumina.

Acknowledgment

J.R.A. and J.H.K. acknowledge partial financial support of this project by the National Science Foundation, Grant No. DMR 73-07507 A02. J.R.A. wishes to express his appreciation to Professor Charles Deportes, I.N.P.G.–E.N.S.E.E.G., Laboratoire d'Energétique et Electrochimique, L.A. 265, Domaine Universitaire-B.P. 44, 38401 Saint Martin D'Hères, France, for sponsorship under the United States–France Exchange of Scientists Program. M. Kleitz, E. Schouler, F. Hartmann-Boutron, and M. Armand are thanked for helpful discussions. Alain Foissy is thanked for help in sample preparation.

References

1. J. P. Boilot, A. Kahn, J. Thery, R. Collongues, J. Antoine, D. Vivien, C. Chevrette, and D. Gourier, *Electrochim. Acta* **22**, 741 (1977).
2. J. Antoine, D. Vivien, J. Thery, R. Collongues, and J. Livage, *J. Solid State Chem.* **21**, 349 (1977).
3. J. Antoine, Ph.D. Thesis, L'Université Pierre et Marie Curie, Paris, October 1976.
4. Y. F. Yu Yao and J. T. Kummer, *J. Inorg. Nucl. Chem.* **29**, 2453 (1967).
5. L. F. Power and A. M. Tait, *Anal. Chem.* **47**, 1721 (1975).
6. R. T. Lewis, *Rev. Sci. Instrum.* **42**, 31 (1971).
7. R. T. Lewis, *Rev. Sci. Instrum.* **44**, 518 (1973).
8. E. B. Sandell, "Colorimetric Determination of Traces of Metals," 3rd ed., Interscience, New York (1972).
9. F. Varret, H. Czeskleba, F. Hartmann-Boutron, and P. Imbert, *J. Phys.* **33**, 549 (1972).
10. H. Annersten and S. Hafner, *Z. Kristallogr.* **137**, 321 (1973).
11. D. L. Wood and J. P. Remeika, *J. Appl. Phys.* **38**, 1038 (1967).
12. E. S. Gaffney, *Phys. Rev. B* **8**, 3484 (1973).
13. P. M. Jaffe, *J. Electrochem. Soc.* **115**, 1203 (1968).
14. F. A. Hummel and J. A. Sarver, *J. Electrochem. Soc.* **111**, 252 (1964).
15. M. I. Bán, J. Czászár, and M. Hegyháti, *J. Mol. Struct.* **19**, 455 (1973).
16. D. T. Palumbo and J. J. Brown, *J. Electrochem. Soc.* **117**, 1184 (1970).
17. J. H. Kennedy and J. R. Akridge, 28th Meeting of the International Society of Electrochemistry, Druzhba near Varna, Bulgaria, 18–23 September 1977.
18. B. N. Figgis, "Introduction to Ligand Fields," Chap. 10, Interscience, New York (1966).
19. B. N. Figgis and J. Lewis, *In* "Progress in Inorganic Chemistry" (F. A. Cotton, Ed.), Vol. 6, p. 37, Wiley (Interscience), New York (1964).
20. A Ernshaw, "Introduction to Magnetochemistry," pp. 34–35, Academic Press, New York (1968).
21. J. H. Kennedy and J. R. Akridge, *J. Amer. Ceram. Soc.* **58**, 279 (1976).
22. J. H. Kennedy and A. F. Sammells, *J. Electrochem. Soc.* **119**, 1609 (1972).
23. W. L. Roth, F. Reidinger, and S. La Placa, "Superionic Conductors" (G. D. Mahan and W. L. Roth, Eds.), pp. 223–241 Plenum Press, New York (1976).
24. T. Kodama and G. Muto, *J. Solid State Chem.* **17**, 61 (1976).
25. W. L. Roth, W. C. Hamilton, and S. J. Laplaca, *Amer. Crystallog. Assoc. Abstr.*, **2**, 1 (1973).
26. P. D. Dernier and J. P. Remeika, *J. Solid State Chem.* **17**, 245 (1976).
27. R. Ingalls, *Phys. Rev.* **133A**, 787 (1964).
28. A. T. Howe and G. J. Dudley, *J. Solid State Chem.* **18**, 149 (1976).